Title

Importance of cell division angle, position of cell proliferative area, and localization of AN3 in lateral organ morphology

Authors

Ayaka Kinoshita[1*], Makiko Naito[1*], Hirokazu Tsukaya[1]

*Contributed equally to this work

Affiliations

[1]Graduate School of Science, The University of Tokyo, Tokyo, Japan

Correspondence

Corresponding Author: Hirokazu Tsukaya

Contact: tsukaya@bs.s.u-tokyo.ac.jp

Word counts & number of figures

Total (main body): 5730 words

Introduction: 993 words

Materials and Methods: 1156 words

Results: 1514 words

Discussion: 2067 words

Number of figures: 11

Number of supporting information: 1

Abstract

Leaf meristem is a cell proliferative zone present in the lateral organ primordia, and it contributes to the expansion of lateral organ lamina. In this study, we investigated how the proliferative zone affects the final morphology of the lateral organs. We examined how cell proliferative zones differ in the primordia of polar –auxin transport inhibitor (PATI)-treated leaves and floral organs from normal foliage leaf primordia of *Arabidopsis thaliana* with focus on the spatial accumulation pattern of mRNA and protein of *ANGUSTIFOLIA3* (*AN3*), a key element for leaf meristem positioning. As a result, we revealed that organ shape change by PATI treatment could not be attributed to changes in leaf-meristem positioning, size of the leaf meristem, or the expression pattern of *AN3*. Instead, it was attributed to altered cell division angles in the leaf meristem. In contrast, different shapes between sepals and petals compared with foliage leaves were observed to be correlated with both altered meristem position associated with altered *AN3* expression patterns and different distributions of cell division angles. These results strongly indicate that lateral organ shapes are regulated via two aspects: position of meristem and cell division angles; the former is mainly governed by the *AN3* expression pattern.

Key words

AN3, cell division, lateral organ, leaf meristem, morphology, polar-auxin-inhibitor

Introduction

The shape of the leaf plays an important role in determining its photosynthetic function. Moreover, the shape of floral organs, which are evolutionarily derived from

leaves, is also important for reproductive success. Therefore, the shape of these lateral organs varies among species to maximize their survival ability in their natural habitats. To understand these variations, it is important to understand their developmental properties.

The center of morphogenesis in plants is the meristem, where active cell division occurs. The shoot apical meristem (SAM) is essential for the production of new above-ground organs. In terms of lateral organs, especially for leaf primordia, the leaf meristem supplies cells to the leaf blade; thus, researchers have investigated the nature of the meristem to understand the morphogenesis of lateral organs (e.g. Esau, 1977; Donnelly *et al*., 1999; Kazama *et al*., 2010; Ichihashi *et al*., 2011).

In many angiosperms, such as *Arabidopsis thaliana*, the leaf meristem is at the base of each leaf (Tsukaya, 2014). Cell proliferation initially occurs throughout the leaf primordium but is restricted to its basal regions as the leaf primordium grows further (Donnelly *et al.*, 1999; Kazama *et al.*, 2010). The control on the restriction of cell proliferation zone is not completely understood, but a transcriptional coactivator called ANGUSTIFOLIA3 (AN3)/GRF-INTERACTING FACTOR1(GIF1) is considered to positively control cell proliferation in leaf primordia; the spatial patterns of AN3/GIF1 accumulation match well the cell proliferation zone, suggesting that AN3/GIF1 may act as an important determinant in positioning the leaf meristem(Horiguchi *et al.*, 2005; Kawade *et al.*, 2017) Cell division angles in the *AN3*-expressing region, except for areas along the margin and vasculature, were observed to be randomized (Yin & Tsukaya, 2016). *AN3* encodes a protein that is homologous to the human synovial sarcoma translocation protein (Horiguchi *et al.*, 2005; Nelissen *et al.*, 2015), and during leaf development, it is expressed at the base of leaf primordia. AN3 protein moves (Kawade *et al.*, 2013) and

forms a gradient along the proximal-distal axis on the leaf, with the leaf base having the highest concentration of AN3 protein (Kawade *et al.*) and thus is involved in the positioning of the leaf meristem. However, how *AN3* expression is controlled within the leaf meristem is still unknown.

AN3 is also involved in the morphogenesis of each floral organ (Lee *et al.*, 2009a, 2014). A petal in the *an3* mutant has a smaller number of cells and a narrower shape than that of the wild type (Lee *et al.*, 2009b), as seen in the foliage leaves, suggesting a common role of AN3 in leaf and floral organ primordia. However, cell proliferation is active in the distal part of the petal primordia and not in the basal part, as in the leaf primordia (Disch *et al.*, 2006; Anastasiou *et al.*, 2007). Thus, if AN3 has the same role in the positional determination of the meristematic zone in petal primordia, AN3 proteins are expected to accumulate apically and not basally in petal primordia; however, no previous studies have examined it. Marginal/apical positioning of meristematic zone in petals may be an ancestral character that is directly comparable to apical positioning of SAM (Boyce, 2007). Although the basal positioning of the leaf meristem is common in angiosperms, marginal/apical positioning in leaf primordia is also known in some ferns and gymnosperms. Therefore, a comparison of leaf primordia with floral organ primordia of the same species, with special emphasis on *AN3* expression, may contribute towards understanding the roles and evolutionary history of differences in the positioning of cell proliferation activity in the primordia of these lateral organs.

The venation pattern is an observed difference between the leaves of angiosperms, ferns, and gymnosperms (Boyce, 2007). In the lateral organs of ferns and gymnosperms harboring meristems along the apical margin, the leaf vein shows a bifurcated pattern and is open at the end. In contrast, lobed and closed patterns are

common in eudicots including *A. thaliana*, and parallel patterns are common in monocots (Dengler & Kang, 2001). Thus, the venation pattern may be important in regulating leaf organogenesis. Mutants with an abnormal venation pattern mostly show altered leaf shapes in *A. thaliana* (Candela *et al.*, 1999). Based on this correlation, an interaction between spatial control of the leaf cell proliferation zone and leaf venation pattern has been suggested (Boyce, 2007).

In vein development in the leaf, biosynthesis and transportation of the plant hormone auxin (indole-3-acetic acid, IAA) plays an important role (Cheng *et al.*, 2006). For example, *GNOM* and *PIN-FORMED* (*PIN*) genes that control polar auxin transport (PAT) (Verna *et al.*, 2019) regulate the vein formation during leaf development. Members of the PIN family have been extensively studied as major factors in PAT, the most famous being PIN1 (Okada *et al.*, 1991). Mutations in many PIN genes induce defects in leaf vein patterns, with wide and bifurcated midveins and altered leaf blade shapes (Sawchuk *et al.*, 2013).

Many PAT inhibitors (PATIs) have been used to examine the role of PAT in plant organogenesis, including 2,3,5-triiodobenzoic acid (TIBA) and N-1-naphthylphthalamic acid (NPA). Through indirect evidence, they bind to the same auxin efflux carriers to inhibit their activity (Teale & Palme, 2018). When plants are treated with PATI, their leaves exhibit abnormal leaf venation patterns, including very thick midveins and marginal veins, similar to that of *pin1* mutants (Sieburth, 1999). In addition, leaf shape becomes rounder and shorter than that of control plants. However, to date, no study has examined the effect of PATI on the cell proliferation pattern in leaf primordia.

To completely understand the morphogenesis process of lateral organs, it is necessary to understand the role of the lateral organ meristem on the final organ shape

and factors that affect the properties of meristems. In this study, we utilized PATI-treated leaves and floral organs as leaves with altered venation patterns or modified leaves and investigated the spatial position of cell proliferative area, cell division angle, and possible factors that control the properties of lateral organ meristems, using AN3 as a key clue.

Materials and Methods

Plant growth

For analysis of the leaf primordia, *A. thaliana* Col-0 (wild type [WT]), or those carrying *CYCLINB1;1*(*CYCB1;1*)::GUS, *an3-4*, *an3-4*/*pAtAN3::AN3-GREEN FLUORESCNT PROTEIN* (*GFP*), *an3-4*/*pAtAN3::AN3-3xGFP*, *gl-s92f*, or *gl-s92f*/*an3* were grown on sterile growth medium that contained 0.5 × Murashige and Skoog medium (MS, Wako, Osaka, Japan), 1% (w/v) sucrose (Nacalai Tesque, Kyoto, Japan), and 0.8% (w/v) agar (Nacalai Tesque, Kyoto, Japan) (Wako, Osaka, Japan) adjusted to pH 5.8 (KOH). Approximately, 1 M PATI (TIBA and NPA) stocks were dissolved in dimethyl sulfoxide and added to the medium to a final concentration of 10 μM. The medium composition was based on that described by Sieburth (1999).

Seeds were sterilized by immersing in a solution of 2% (v/v) Plant Preservative Mixture™ (Plant Cell Technology, Washington, D.C., USA), 0.1% (v/v) Triton X-100 (Nacalai Tesque, Kyoto, Japan), and 50 mg/L $MgSO_4$ for 6 h or a solution of 10% (v/v) sodium hypochlorite (Nacalai Tesque, Kyoto, Japan) and 1% (v/v) Triton X-100 for 5 min and twice with sterile water prior to plating. The plates were incubated at 24°C under constant illumination.

For analyses of the floral organ primordia, *A. thaliana* Col-0 and *an3-4*/*pAtAN3::AN3-1xGFP* (Kawade *et al.*, 2013) were sown on rockwool (Toyobo, Osaka,

144 Japan) and grown under white fluorescent light conditions (ca. 40 μmol m^{-2} s^{-1}) at 22–
145 23°C supplied with water containing 1 g/L powder Hyponex (Hyponex, Osaka, Japan).
146
147 GUS experiments
148 Detection of β-glucuronidase (GUS) activity was carried out using 5-bromo-4-
149 chloro-3-indolyl-β-D-glucuronide (X-Gluc) as a substrate. Plant tissue was first placed in
150 90% (v/v) acetone on ice for 10 min, washed with sodium phosphate buffer (pH 7.0), and
151 then placed in X-Gluc buffer solution (0.5 mg/mL X-Gluc, 100 mM $NaPO_4$ (pH 7.0), 5
152 mM $K_3Fe(CN)_6$, 5 mM $K_4Fe(CN)_6$, 10 mM EDTA, 0.1% (v/v) Triton X-100) under
153 vacuum for 15 min or more and then placed in the dark at room temperature (ca. 20°C).
154 After GUS detection, plant tissues were rinsed in 70% (v/v) ethanol and fixed in
155 ethanol: acetic acid (6:1) solution. After chlorophyll was removed, the tissue was
156 preserved in 70% EtOH in the dark. Plant tissues were mounted on slides with chloral
157 hydrate solution (50 g chloral hydrate, 5 g glycerol, 12.5 mL distilled water) (Tsuge *et al.*,
158 1996) and observed under a microscope after the tissue became transparent enough.
159
160 AN3-GFP observations
161 Leaf primordia (5 days after sowing stage: DAS) and flower primordia of *A.*
162 *thaliana an3-4*/*pAN3::AN3-GFP* and *an3-4*/*pAN3::AN3-3xGFP* lines were fixed in 4%
163 (v/v) paraformaldehyde (PFA) in phosphate-buffered saline (PBS) with 0.05% (v/v)
164 Triton X-100 by immersing them in the fixation mixture, deairing them for 10 min (for
165 leaf primordia) or 15 min (twice, for flower primordia) and placed at 4°C overnight.
166 The samples were then washed in PBS (10 min, twice) and stored in PBS at room
167 temperature for leaf primordia and at 4°C for flower primordia until observation.

168 The samples were then dissected using a sharp razor under the microscope. Leaf
169 primordia were mounted on slides with PBS and observed under a confocal microscope
170 (FV3000; Olympus, Tokyo, Japan) with a GFP filter for leaf primordia and an upright
171 fluorescent microscope (DM4000; Leica Microsystems GmbH, Wetzlar, Germany) for
172 floral organ primordia.
173
174 Data analysis on the position of leaf meristem and the arrest front
175 This method was derived from Kazama *et al*. (2010) and Ikeuchi *et al.* (2011).
176 This method is used to determine the position of the leaf meristem. First, an image of a
177 leaf with a GUS expression pattern was prepared. The outer region of leaf was cropped,
178 and the image was rotated so that the leaf base was on the left side of the image. Then,
179 the blue region was extracted, and a binary image was created using ImageJ
180 (https://imagej.nih.gov/ij/). The number of white pixels was counted for each column, and
181 the arrest front was determined based on the definition of the point at which the ratio of
182 white pixels was half that of the maximum and farthest from the blade base. The distance
183 from the leaf base of each arrest front point was plotted for each condition in a box plot.
184 Statistical analysis was performed using the R software.
185 Similarly, the arrest front position was determined as following; first, a series of
186 z-stack images were stacked using ImageJ software. Stacked images with the outer side
187 of the leaf were cropped and rotated so that the leaf base was on the left side of the image.
188 The region with GFP fluorescence was extracted, and from this image, a binary image
189 was created. The number of black pixels was counted in each column. The arrest front
190 was determined based on the definition of the point at which the ratio of black pixels was
191 half that of the maximum and farthest from the blade base. The distance from the leaf

192 base of each arrest front point was divided by the leaf length because of the size difference
193 between lines. The obtained data were plotted for each condition in a box plot. Statistical
194 analysis was performed using the R software.
195
196 Observation of Aniline Blue signal
197 This method was derived from previous studies for the detection of newly
198 formed cell walls (Kuwabara & Nagata, 2006; Kuwabara *et al.*, 2011). Leaf primordia (7
199 DAS) of *A. thaliana gl1(glabra1)-s92f* and *gl1-s92f/an3-4* mutants and Col-0 flower
200 petals and sepals were first fixed in a mixture of ethanol and acetic acid (4:1, v/v) for 30
201 min and then rinsed in 100% ethanol. Then, the samples were immersed in a mixture of
202 ethanol and 100 mM phosphate buffer (pH 9.0; 1:1, v/v) for 30 min and then in 100 mM
203 phosphate buffer (pH 9.0) for 10 min. Finally, the samples were immersed in a 0.02%
204 (w/v) solution of aniline blue in 100 mM phosphate buffer (pH 9.0) for at least 7 days and
205 up to 30 days at 4°C. Leaf primordia were mounted on slides with the staining solution
206 and observed under a confocal microscope (FV10C-PSU; Olympus, Tokyo, Japan) under
207 UV excitation with a DAPI (4',6-diamidino-2-phenylindole) filter. The data were
208 analyzed by taking each angle of the septum wall. Calculations were performed using
209 Microsoft® Excel.
210
211 Observation of EdU-marked cells
212 We used the Click-iT EdU Alexa Fluor 488 Imaging Kit (Thermo Fischer
213 Scientific, Waltham, MA, USA) to visualize the cells in S phase. We dissected the
214 inflorescence of *A. thaliana* into several pieces and soaked the flower clusters into 10 μM
215 5-ethynyl-2'-deoxyuridine (EdU) solution in 1/2 MS medium with 1% sucrose for 3 h

under ~45 μmol m^{-2} s^{-1} white fluorescent light. The samples were washed with PBS containing 0.1% Triton X-100 and fixed with FAA (37% [v/v] formaldehyde, 5% [v/v] acetic acid, 50% [v/v] ethanol) and stored at 4°C. Subsequent fluorescent labeling with Alexa Fluor 488 or 555 (Thermo Fischer Scientific, Waltman, MA, USA) was conducted according to the manufacturer's instructions. Floral organs were mounted on slides, and fluorescent dye signals conjugated to EdU were observed under fluorescent microscope (DM4000; Leica Microsystems GmbH, Wetzlar, Germany).

Results

Change in the length of cell proliferation zone

In the PATI-treated plants, the leaves were shorter and rounder than those of the control plants (Fig. **1D-F**, Fig. **2**). The leaf vein pattern also differed in PATI-treated leaves (Fig. **1D-F**, Fig. **2**); namely, the midvein was widened and bifurcated, the lateral veins ran parallel to each other, and the veins adjacent to leaf margins were also widened. These observations are consistent with those of previous reports (Mattsson *et al.*, 1999; Sieburth, 1999; Sawchuk *et al.*, 2013).

To investigate the effect of inhibition of PAT on the leaf meristem, the cell proliferation zone was observed in the leaf primordia of PATI-treated plants. The *CYCB1;1::GUS* line is used to visualize dividing G2-M phase cells (Donnelly *et al.*, 1999). The first and second rosette leaves of 6-DAS seedlings for control plants and 7-day-old seedlings for PATI-treated plants were used for this experiment, considering the growth retardation observed in the PATI-treated plants.

In the PATI-treated plants, the cell proliferation zone remained in the proximal position, similar to the control plants (Fig. **1A-C**). The images were processed to further

examine the positioning of the cell proliferation zone (Fig. **3**). We observed that both the length of the cell proliferation zone from the leaf base and the total ratio of cell proliferation zone to the total leaf length were found to be increased in PATI-treated leaves (Fig. **4**).

AN3 mRNA and AN3 protein localization in leaf primordia

To investigate how the length of the cell proliferation zone increased, we examined the localization of *AN3*, a positive regulator of cell proliferation. As AN3 protein can move between cells, two lines, *an3-4/pAtAN3::AN3-GFP* and *an3-4/pAtAN3::AN3-3xGFP*, were used for the observation. The former can detect actual protein localization, whereas the latter is used to monitor mRNA localization because it represents accumulation of the protein without cell-to-cell movement ability (Kawade *et al.*, 2013, 2017). The first and second rosette leaves of 5 DAS seedlings were used for this experiment.

We observed that the overall localization of AN3 under PATI treatment did not change from that of the control; it remained in the proximal region (Fig. **5**). This confirms the observation in the cell proliferation zone described above. The *AN3*-expressing regions were also determined using the same image processing method used for the analysis of cell proliferation zone. As a result, the *AN3*-mRNA expressing regions were slightly longer in the PATI-treated leaves than in control; in NPA-treated leaves, significant differences were detected compared with that of the control. However, protein localization did not show a statistical difference between TIBA- and NPA-treated plants (Fig. **6**). Therefore, even though changes in *AN3* mRNA expression pattern may influence the increase in length in the cell proliferation regions, the spatial gradient of AN3 protein

264 along the longitudinal axis of leaf primordia did not change. Thus, the influence of PATI
265 treatment on the AN3 protein accumulation pattern is rather limited.

266 In contrast, when *an3-4*/*pAtAN3::AN3-3xGFP* were treated with PATI, we
267 recognized that *AN3* localization was missing in the vasculature region. This missing
268 localization was also observed in control conditions, but in PATI-treated leaves, the
269 vasculature was very thick, and therefore, the absence was recognizable (Fig. **1D-F**, Fig.
270 **5**).

271

272 Cell division angles in leaves

273 Based on the changes in the size or pattern of the cell proliferation zone, the
274 observed leaf-shape change by PATI treatment could not be explained. Analysis of cell
275 division angles was performed to further investigate how it affects organ shape under
276 PATI treatment. We used the *gl1-s92f* mutant and *gl1-s92f*/*an3-4* double mutants for this
277 experiment. We used *gl1-s92f* mutants that lacked trichomes as a control, because
278 trichomes obstruct cell division plane observation using aniline blue staining. The angles
279 were determined against the proximal-distal axis, starting from the leaf base and parallel
280 to the midvein for the first and second rosette leaves of 7 DAS seedlings (Fig. **8**; Fig. **S1**).

281 As a result, a variety of cell division angle patterns were observed (Fig. **7A**, **B**,
282 Fig. **8**). In the control plants, the cell division angle occurred around 130°–140° (Fig. **7A**).
283 In PATI-treated leaves, this peak was less evident, and cell division was likely to occur in
284 all directions (Fig. **7A**). This may have contributed to changes in leaf shape, with rounder
285 and shorter leaves, when treated with PATI (Fig. **1D-F**, Fig. **2**).

286 Cell division angle investigation was also performed in the *an3-4* mutant plants.
287 In the *an3-4* mutant without PATI, the peak of cell division angle was around 140–150°,

288 which differed from that of the control condition (Fig. **7A, B**), suggesting that AN3 might
289 shift the cell division angle to smaller angles, that is, a shift from proximo-distal to medio-
290 lateral direction. In the *an3* mutant treated with PATI, however, the distribution of cell
291 division angle became similar to that of WT plants treated with PATI (Fig. **7A, B**). This
292 suggests that the randomizing effect of PATI on cell division angle is superior to that of
293 the *an3* genotype of the plant biasing cell division angle to the proximo-distal axis. In
294 addition, there was a specific pattern change in the cell division angle of each PATI type
295 (TIBA and NPA).
296
297 <u>The position of cell proliferative area in floral organs</u>
298 Although floral organs such as sepals, petals, stamens, and carpels are homeotic
299 to leaves, their shapes are absolutely different. Even between sepals and petals, both of
300 which are planar organs, there are distinct differences in shape in *A. thaliana*. In the distal
301 part, the sepal is narrower, and the petal is wider. In this aspect, foliage leaves are
302 narrower in the distal part, similar to sepals.
303 We observed cell proliferation patterns in floral organ primordia to investigate
304 whether these patterns might influence the difference in the final organ shape. To visualize
305 dividing cells in floral organs, we used EdU. In a sepal, cell division was observed in the
306 basal part of the organ primordia through the observed developmental stages (Fig. **10**),
307 which resembled to that in leaves. In contrast, cell division in the petal primordia was
308 observed in whole organ when the organ was around 100–150 μm in length, and the distal
309 and marginal regions when the organ was around 400 μm in length (Fig. **10**), which
310 marked a clear difference from that of leaves and sepals. A similar tendency was also
311 observed in the aniline-blue-stained samples (Fig. **9**).

AN3 protein localization in floral organs

As AN3 is a key regulator of the leaf meristem position, and it promotes the cell division of petals and sepals, we suspected that AN3 protein accumulation patterns may be different between them, which have different positions of the cell proliferative area. AN3-GFP signals were only observed in the basal part of sepal organ primordia, whereas the signals were observed in the distal region through the observed developmental stages in petal organ primordia. Moreover, in terms of petal primordia, sparse signals were also observed in the central region and the basal part in the later stage 9 (Fig. **10**), where EdU signals were rarely observed.

Phenotype of *an3* mutant in sepal

It is reported that *an3* mutants have narrower petals and lesser number of cells than that of the WT (Horiguchi *et al.*, 2005; Lee *et al.*, 2009a); the sepal phenotype has not been investigated. In order to investigate whether AN3 maintains leaf meristem in sepal primordia, which was suggested by the AN3 protein accumulation pattern and proliferative area, we compared the phenotype of *an3-4* and the WT in the sepals (Fig. **11A–B**). The area of the organ was smaller in *an3* than in the WT (Fig. **11C**), and we also observed that the *an3* mutant had less complex veins as compared to that of the WT, which was evaluated based on the number of secondary and higher veins in the m-shaped or two n-shaped primary veins (Fig. **11C, D**).

Cell division angles in floral organs

To observe the influence of cell division angle on the final shape of floral organs, cell division angle analysis was conducted in the sepals and petals. Flowers at stages 8–10 were used in this experiment to observe active cell proliferation (Alvarez-Buylla *et al.*, 2010).

The cell division angle in floral organs peaked at approximately 60°–90° and 140°–180° (Fig. **8**). This twin peak pattern is different from the cell division angle in leaves, which only had one peak (Fig. **7A, B**). Because sepals and leaves had similar localization of the cell proliferation zone, we expected that the distribution of cell-division angles would be similar, but on the contrary, the overall tendency of cell division in sepals was similar to that of petals. This suggests that the pattern of cell division angles is not associated with the localization of the cell proliferation zone but with organ identity.

The cell divisions with the 60°–90° peak, which were divisions in the mediolateral direction of the primordia, were identified mostly in the central regions of the petal primordia. In contrast, the divisions that corresponded to the 140°–180° peak, which were divisions in the proximo-distal direction, were identified mostly in the marginal regions of the petal primordia (Fig. **9**).

Discussion

In this study, we examined how cell proliferative zones differ in the primordia of PATI-treated leaves and floral organs from normal foliage leaf primordia of *A. thaliana* with focus on the spatial expression pattern of *AN3*, a key element for leaf meristem positioning (Kawade *et al.*, 2010). As a result, we revealed that organ shape change by PATI treatment cannot be attributed to changes in leaf-meristem positioning, size of the

leaf meristem, or the expression pattern of *AN3* and is rather attributed to altered cell division angles in the leaf meristem. In contrast, different shapes of sepals and petals compared with foliage leaves were found to be correlated with both altered meristem position associated with altered *AN3* expression patterns and different distributions of cell division angles. These results strongly indicate that lateral organ shapes are regulated via two aspects: position of meristem and cell division angles; the former is mainly governed by the *AN3* expression pattern. In the following sections, several aspects of the above findings are discussed.

The position of leaf meristem in PATI-treated plants

When *A. thaliana* plants were treated with PATI, the cell proliferation zone in leaf primordia did not show any changes in terms of localization. However, both the length of the cell proliferation zone in leaf primordia and the ratio of the cell proliferation zone occupying the primordia were observed to be increased (Fig. **4**). As previously reported (Sieburth, 1999), PATI-treated leaves were rounder and shorter, whereas a longer proliferation zone would be expected to produce a longer leaf. Instead, changes in the cell division angles could be attributed to the altered leaf shape.

In this study, it was observed that even when PAT was inhibited, there was no change in the basal expression pattern of *AN3* (Fig. **5**). The *AN3* mRNA expression zone was slightly expanded to the distal direction in the expression zone ratio, although the actual length was not significantly different (Fig. **6**). Indeed, the final AN3 protein distribution remained unchanged under PATI treatment (Fig. **6**). Moreover, the results for NPA and TIBA showed the different trend; while TIBA increased the mRNA localization zone and protein localization of AN3, NPA increased *AN3* mRNA localization zone but

382 did not affect protein localization of AN3. In either case, *AN3* mRNA expression and AN3
383 protein diffusion were not regulated by auxin.

384 We also observed that *AN3* was not expressed in leaf veins (Fig. **5**). This trend
385 was seen in PATI-treated leaves as well as in control conditions; however, it was not
386 evident because the veins in control conditions were much thinner than those of PATI-
387 treated leaves (Fig. **1D-F**). This may happen if *AN3* expression is shut down in
388 differentiated vascular cells, which may imply that the vasculature differentiation by
389 auxin is superior to cell proliferation maintenance by AN3.

390

391 Cell division angle and leaf shape

392 A longer proliferation zone is expected to make a longer leaf; however, in PATI
393 treatment, it produced shorter leaves. The cell division is also an important factor in both
394 leaf development and leaf vein architecture (Kang *et al.*, 2007). In this study, analysis of
395 the cell division angle revealed that the pattern differed between PATI-treated plants (Fig.
396 **7A**). This difference in the pattern could be a cause for the differences in leaf shape.
397 Namely, in comparison with control leaf primordia that had major division angles in
398 130°–140°, PATI-treated leaf primordia had dispersed division angles in many directions,
399 forming a round and short leaf, which matched the phenotype (Fig. **1D-F**, Fig. **3**). We
400 observed the *an3* mutant tended to divide around 140°–150°, which partially explains the
401 narrow leaf phenotype of *an3* mutants, as cell division along the proximal-distal axis was
402 increased.

403

Determining cell division angle in leaves

In this study, there were two components that changed the cell division angle: PAT and AN3. When PAT was inhibited, the peak in the cell division angle distribution became less evident (Fig. **7A**). As auxin flow controls vascular cell polarity (Linh *et al.*, 2018), and plays a role in cell division angle (Yin & Tsukaya, 2016), it is possible that the cells divide in the direction of auxin flow. In contrast, both NPA and TIBA affect actin dynamics (Teale & Palme, 2018; Zou *et al.*, 2019) that can affect cytoskeletal regulation of cytokinesis, and may be one of the underlying reasons for the change in cell division angle.

Additionally, in the *an3* mutant, cell division along the proximal-distal axis accounted for a larger proportion of cells than that in the WT (Fig. **7B**). The increase in cell division along the proximal-distal axis may be due to changes in the overall direction of cell division during leaf development. In a previous report, the phase of cell division was divided into two phases: the first has more divisions along the proximal-distal axis than the second phase (Horiguchi *et al.*, 2011). Furthermore, in *an3* mutants, the transition from the first to the second phase does not occur before the termination of cell division activity (Horiguchi *et al.*, 2011). The shift in the peak of the cell division angle observed in the *an3* mutant reflects this failure in shifting to the second phase of cell proliferation, which confirms the results of previous studies. Therefore, AN3 functions in the transition to second phase of cell division, and as a result, cells divide along the proximal-distal axis in the absence of AN3. More precisely, AN3 might promote the shift of the cell division angle from the proximo-distal to medio-lateral direction.

In addition, in *an3* mutants treated with PATI, the cell division angles were similar to those of WT treated with PATI (Fig. **7A, B**). This suggests that the randomizing

effect of PATI on cell division angle is superior to that of AN3 and that the loss of PAT results in cell division in random directions irrespective of the presence or absence of AN3.

Position of meristematic tissue determines the final floral organ shape

The final organ shape is determined by various factors, such as acceleration and deceleration of proliferation, oriented cell division and expansion, and the meristem position (Tsukaya, 2018). In this study, we showed that the position of the cell proliferative area was completely different between sepals and petals, which are morphologically different. The petal of *A. thaliana* with a modest fan shape has a proliferative region in the distal part, which is similar to ferns with fan-shaped morphology that is rare in angiosperm leaves, coinciding with leaf meristem at the apical margin (Boyce, 2007; Tsukaya, 2014, 2018). This suggests that the morphological differences between sepals and petals could be partly explained by the meristematic position in each organ.

Although predominant cell division occurs in submarginal plate meristem to widen the leaf blade area in leaf primordia (e.g., Poethig and Sussex, 1985), it was also shown that marginal meristem residing in the margin of the primordia also exists (Alvarez *et al.*, 2016). Alvarez et al. (2016) showed that when NGATHA and CINCINNATA-class-TCP were knocked down, indeterminate marginal growth occurred in the entire margin of the leaf blade, suggesting potential meristem activity in this area. Interestingly, marginal growth occurs only in the distal region of floral organs, including sepals and petals. Although in our experiments, active cell division occurred in the proximal part of the sepal primordia, it is possible that the potential marginal meristem in the distal part

452 also contributes to the elaborate final shape of the sepal (Floyd & Bowman, 2010). In
453 terms of petals, active cell division occurs in the distal margin in the first place; therefore,
454 the marginal meristem may contribute more than leaves or sepals. Since the activity of
455 meristem in the distal marginal area of a blade has been discussed as an ancestral character
456 (Floyd & Bowman, 2010), petals may retain this developmental character (Boyce, 2007).
457 We observed EdU signals in the entire margin of the petal primordia at least until the
458 organ size was 400 μm in length, even in the proximal region. Considering the results of
459 Alvarez et al. (2016) on leaf primordia, the nature of proliferative cells in marginal areas
460 is different among different organs.
461
462 Determining factors for the meristematic position
463 Several key genes are known to positively control cell proliferation in the leaf
464 meristem (Nakata *et al.*, 2012; Ichihashi & Tsukaya, 2015). Among them, the AN3-
465 protein-accumulated region matches well with the cell proliferative area in leaf primordia
466 (Kawade *et al.*, 2017), suggesting that AN3 is an important determinant of the leaf
467 meristem position. Moreover, the smaller size of a petal in *an3* or triple knockdown of
468 the GIF family (Kim & Kende, 2004; Horiguchi *et al.*, 2005; Lee *et al.*, 2009a) suggested
469 that AN3 is also involved in the promotion of cell proliferation in the petal. However, its
470 functioning zone in primordia has not been well investigated. In this study, we showed
471 that AN3-expressed region overlapped well with the cell proliferative area in both sepals
472 and petals, as observed in leaf primordia. In addition, we first showed that sepals in *an3*
473 mutants are likely to have a smaller number of cells as petals or foliage leaves. These
474 results strongly suggest that AN3 functions as a determinant of the meristematic position
475 and activity in floral organs. In the past, JAGGED (JAG) was examined as a candidate

of a regulatory gene for the specific morphology in the Arabidopsis petal differed from leaves, from the following points: the loss-of-function *jag* mutant has narrower and shorter petals, the *JAG* over-expressor has larger petals; its mRNA is expressed distal margin (Sauret-Güeto et al. 2013). At that time point JAG was the only one candidate 'organizer' that gives the petal with a pattern of growth orientations that fans out. But now AN3 became to be an additional candidate that fulfils the required, above-mentioned conditions. Indeed *AN3* was identified as a direct target of JAG (Schiessl *et al*. 2014). The role of AN3 as the 'organizer' should be examined carefully in the future.

However, in terms of petal primordia, AN3 protein signals were also observed in the less proliferative area. This might be due to a lack of associating transcriptional factors such as GROWTH REGULATING FACTOR5 (GRF5), which is necessary to promote cell proliferation in leaf primordia (Horiguchi et al., 2005), in such regions. Alternatively, because signals in the proximal part were not as strong as those in the distal region, the concentration of AN3 proteins might not be enough to promote cell division to the extent that EdU was incorporated.

The regulation of meristem position floral organ identity genes needs to be investigated (Coen and Meyerowitz, 1991). Honma and Goto (2001) and Pelaz et al. (2001) revealed that when A genes (*APELATA1*) and B genes (*APELATA3* and *PISTILATA*) were ectopically expressed together with *SEPALLATA2/3* in rosette leaves, the rosette leaves obtained petal identity, and the color and cell shape became petal-like. However, the overall organ shape has not yet been investigated in detail. From our results, the transformed organ is not fan-shaped, but has a taper off shape, which is similar to rosette leaves, cauline leaves, and sepals. This suggests that factors other than the floral

499 identity homeotic genes control the final organ shape. Revealing the mechanisms of *AN3*
500 expression control might shed light on this possibility.

501 The leaves of some gymnosperms and ferns are considered to grow from the
502 meristem in the distal margin. The positioning of these meristems may also be
503 determined by the spatial distribution of leaf meristem-controlling genes such as
504 *AN3/GIF1*. As *GIF* family genes exist in most eukaryotic organisms, including the basal
505 land plants, *Marchantia polymoprha*, *Physcomitrium patens*, and *Sellaginella*
506 *moellendorffi* (Kim and Tsukaya, 2015), further analyses of the *GIFs* in gymnosperms
507 and ferns will answer this question.

508

509 Determining cell division angle in floral organs

510 In this study, the cell division pattern in floral organ primordia was investigated
511 for its possible roles in each floral organ morphology, and both the petals and sepals
512 showed a pattern with twin peaks in the distribution of cell division angles, which was
513 different from that of leaf primordia that had only a single peak (Fig. 8). Although both
514 sepal and leaf primordia have a cell proliferation zone in the basal region, the cell division
515 angle was controlled differently, which may imply that cell division angles depend on
516 organ identity and affect their final shapes.

517 In the petal, the cell division occurred at 60°–90° angle in the central regions,
518 and the cell division with the 140°–180° angle was mostly in the marginal regions,
519 whereas such a pattern was not seen in the sepals (Fig. **9**). This difference may cause
520 differences in shape between sepals and petals, and petal shape, with the distal part being
521 wider than the proximal part, may be caused by the cell divisions that contribute to width
522 in the marginal regions. Thus, we revealed that lateral organ shapes are regulated by two

523 factors: the position of the cell proliferative zone governed by the spatial expression
524 pattern of *AN3* and cell division angles. Even in one species, by changing these two
525 factors, a variety of lateral organ shapes could be realized.
526
527 **Acknowledgments**
528 We would like to thank MEXT and the Graduate Program for Leaders in Life Innovation
529 (GPLLI)/World-leading Innovative Graduate Study Program for Life Science and
530 Technology (WINGS-LST) of the University of Tokyo for providing microscope facilities.
531
532 **Author Contributions**
533 AK, MN, and HT designed the experiments; AK and MN performed the experiments and
534 analyzed the data; AK, MN, and HT wrote the manuscript.
535
536 **Funding**
537 This research was supported by a Grant-in-Aid for JSPS Fellows (AK, #19J14140) and a
538 Grant-in-Aid for Scientific Research on Innovation Areas (HT, #25113002 and
539 19H05672) from MEXT and GPLLI/WINGS-LST of the University of Tokyo (AK).
540
541 **Conflict of Interest**
542 No conflict of interest.
543
544 **Data Availability**
545 Data available on request from the authors.
546

References

Alvarez-Buylla ER, Benítez M, Corvera-Poiré A, Chaos Cador Á, de Folter S, Gamboa de Buen A, Garay-Arroyo A, García-Ponce B, Jaimes-Miranda F, Pérez-Ruiz R V., *et al.* 2010. Flower Development. *The Arabidopsis Book* **8**: e0127.

Alvarez JP, Furumizu C, Efroni I, Eshed Y, Bowman JL. 2016. Active suppression of a leaf meristem orchestrates determinate leaf growth. *eLife* **5**: e15023.

Anastasiou E, Kenz S, Gerstung M, MacLean D, Timmer J, Fleck C, Lenhard M. 2007. Control of plant organ size by KLUH/CYP78A5-dependent intercellular signaling. *Developmental Cell* **13**: 843–856.

Boyce CK. 2007. Mechanisms of laminar growth in morphologically convergent leaves and flower petals. *International Journal of Plant Sciences* **168**: 1151–1156.

Candela H, Martínez-Laborda A, Luis Micol J. 1999. Venation pattern formation in *Arabidopsis thaliana* vegetative leaves. *Developmental Biology* **205**: 205–216.

Cheng Y, Dai X, Zhao Y. 2006. Auxin biosynthesis by the YUCCA flavin monooxygenases controls the formation of floral organs and vascular tissues in Arabidopsis. *Genes and Development* **20**: 1790–1799.

Coen ES, Meyerowitz EM. 1991. The war of the whorls: genetic interactions controlling flower development. *Nature* **353**: 31–37.

Dengler N, Kang J. 2001. Vascular patterning and leaf shape. *Current Opinion in Plant Biology* **4**: 50–56.

Disch S, Anastasiou E, Sharma VK, Laux T, Fletcher JC, Lenhard M. 2006. The E3 ubiquitin ligase BIG BROTHER controls Arabidopsis organ size in a dosage-dependent manner. *Current Biology* **16**: 272–279.

571 **Donnelly PM, Bonetta D, Tsukaya H, Dengler RE, Dengler NG**. **1999**. Cell cycling
572 and cell enlargement in developing leaves of *Arabidopsis*. *Developmental Biology* **215**:
573 407–419.
574 **Esau K**. **1977**. *Anatomy of Seed Plants, 2nd Edition*. New York: John Wiley & Sons.
575 **Floyd SK, Bowman JL**. **2010**. Gene expression patterns in seed plant shoot meristems
576 and leaves: Homoplasy or homology? *Journal of Plant Research* **123**: 43–55.
577 **Horiguchi G, Kim GT, Tsukaya H**. **2005**. The transcription factor AtGRF5 and the
578 transcription coactivator AN3 regulate cell proliferation in leaf primordia of
579 *Arabidopsis thaliana*. *Plant Journal* **43**: 68–78.
580 **Horiguchi G, Nakayama H, Ishikawa N, Kubo M, Demura T, Fukuda H, Tsukaya**
581 **H**. **2011**. *ANGUSTIFOLIA3* plays roles in adaxial/abaxial patterning and growth in leaf
582 morphogenesis. *Plant and Cell Physiology* **52**: 112–124.
583 **Ichihashi Y, Kawade K, Usami T, Horiguchi G, Takahashi T, Tsukaya H**. **2011**.
584 Key proliferative activity in the junction between the leaf blade and leaf petiole of
585 Arabidopsis. *Plant Physiology* **157**: 1151–1162.
586 **Ichihashi Y, Tsukaya H**. **2015**. Behavior of leaf meristems and their modification.
587 *Frontiers in Plant Science* **6**: 1–8.
588 **Ikeuchi M, Yamaguchi T, Kazama T, Ito T, Horiguchi G, Tsukaya H**. **2011**.
589 ROTUNDIFOLIA4 regulates cell proliferation along the body axis in arabidopsis shoot.
590 *Plant and Cell Physiology* **52**: 59–69.
591 **Kang J, Mizukami Y, Wang H, Fowke L, Dengler NG**. **2007**. Modification of cell
592 proliferation patterns alters leaf vein architecture in Arabidopsis thaliana. *Planta* **226**:
593 1207–1218.

Kawade K, Horiguchi G, Tsukaya H. 2010. Non-cell-autonomously coordinated organ size regulation in leaf development. *Development* **137**: 4221–4227.

Kawade K, Horiguchi G, Usami T, Hirai MY, Tsukaya H. 2013. ANGUSTIFOLIA3 signaling coordinates proliferation between clonally distinct cells in leaves. *Current Biology* **23**: 788–792.

Kawade K, Tanimoto H, Horiguchi G, Tsukaya H. 2017. Spatially different tissue-scale diffusivity shapes ANGUSTIFOLIA3 gradient in growing leaves. *Biophysical Journal* **113**: 1109–1120.

Kazama T, Ichihashi Y, Murata S, Tsukaya H. 2010. The mechanism of cell cycle arrest front progression explained by a *KLUH/CYP78A5*-dependent mobile growth factor in developing leaves of *Arabidopsis thaliana*. *Plant and Cell Physiology* **51**: 1046–1054.

Kim JH, Kende H. 2004. A transcriptional coactivator, AtGIF1, is involved in regulating leaf growth and morphology in *Arabidopsis*. *Proceedings of the National Academy of Sciences of the United States of America* **101**: 13374–13379.

Kuwabara A, Backhaus A, Malinowski R, Bauch M, Hunt L, Nagata T, Monk N, Sanguinetti G, Fleming A. 2011. A shift toward smaller cell size via manipulation of cell cycle gene expression acts to smoothen arabidopsis Leaf Shape. *Plant Physiology* **224**: 761–770.

Kuwabara A, Nagata T. 2006. Cellular basis of developmental plasticity observed in heterophyllous leaf formation of Ludwigia arcuata (Onagraceae). *Planta* **224**: 761–770.

Lee BH, Ko JH, Lee S, Lee Y, Pak JH, Kim JH. 2009a. The Arabidopsis *GRF-INTERACTING FACTOR* gene family performs an overlapping function in determining

617 organ size as well as multiple developmental properties. *Plant Physiology* **151**: 655–
618 668.
619 **Lee BH, Ko JH, Lee S, Lee Y, Pak JH, Kim JH**. **2009b**. The Arabidopsis GRF-
620 Interacting Factor gene family performs an overlapping function in determining organ
621 size as well as multiple. *Plant Physiology* **151**: 655–668.
622 **Lee BH, Wynn AN, Franks RG, Hwang Y sic, Lim J, Kim JH**. **2014**. The
623 arabidopsis thaliana GRF-interacting factor gene family plays an essential role in
624 control of male and female reproductive development. *Developmental Biology* **386**: 12–
625 24.
626 **Linh NM, Verna C, Scarpella E**. **2018**. Coordination of cell polarity and the
627 patterning of leaf vein networks. *Current Opinion in Plant Biology* **41**: 116–124.
628 **Mattsson J, Sung ZR, Berleth T**. **1999**. Responses of plant vascular systems to auxin
629 transport inhibition. *Development* **126**: 2979–2991.
630 **Nakata M, Matsumoto N, Tsugeki R, Rikirsch E, Laux T, Okada K**. **2012**. Roles of
631 the middle domain-specific *WUSCHEL-RELATED HOMEOBOX* genes in early
632 development of leaves in *Arabidopsis*. *Plant Cell* **24**: 519–535.
633 **Nelissen H, Eeckhout D, Demuynck K, Persiau G, Walton A, van Bel M, Vervoort**
634 **M, Candaele J, De Block J, Aesaert S, *et al.* 2015**. Dynamic changes in
635 ANGUSTIFOLIA3 complex composition reveal a growth regulatory mechanism in the
636 maize leaf. *Plant Cell* **27**: 1605–1619.
637 **Okada K, Ueda J, Komaki MK, Bell CJ, Shimura Y**. **1991**. Requirement of the auxin
638 polar transport system in early stages of *Arabidopsis* floral bud formation. *The Plant*
639 *Cell* **3**: 677–684.

Pelaz S, Gustafson-Brown C, Kohalmi SE, Crosby WL, Yanofsky MF. **2001**. *APETALA1* and *SEPALLATA3* interact to promote flower development. *The Plant Journal* **26**: 385–394.

Poethig RS, Sussex IM. **1985**. The cellular parameters of leaf development in tobacco: a clonal analysis. *Planta* **165**: 170–184.

Sawchuk MG, Edgar A, Scarpella E. **2013**. Patterning of leaf vein networks by convergent auxin transport pathways. *PLoS Genetics* **9**: e1003294.

Sieburth LE. **1999**. Auxin is required for leaf vein pattern in Arabidopsis. *Plant Physiology* **121**: 1179–1190.

Teale W, Palme K. **2018**. Naphthylphthalamic acid and the mechanism of polar auxin transport. *Journal of Experimental Botany* **69**: 303–312.

Tsuge T, Tsukaya H, Uchimiya H. **1996**. Two independent and polarized processes of cell elongation regulate leaf blade expansion in *Arabidopsis thaliana* (L) Heynh. *Development* **122**: 1589–1600.

Tsukaya H. **2014**. Comparative leaf development in angiosperms. *Current Opinion in Plant Biology* **17**: 103–109.

Tsukaya H. **2018**. Leaf shape diversity with an emphasis on leaf contour variation, developmental background, and adaptation. *Seminars in Cell and Developmental Biology* **79**: 48–57.

Verna C, Ravichandran SJ, Sawchuk MG, Linh NM, Scarpella E. **2019**. Coordination of tissue cell polarity by auxin transport and signaling. *eLife* **8**: e51061.

Yin X, Tsukaya H. **2016**. A pulse-chase strategy for EdU labelling assay is able to rapidly quantify cell division orientation. *The New phytologist* **211**: 1462–1469.

663 **Zou M, Ren H, Li J**. **2019**. An auxin transport inhibitor targets villin-mediated actin

664 dynamics to regulate polar auxin transport. *Plant Physiology* **181**: 161–178.

665

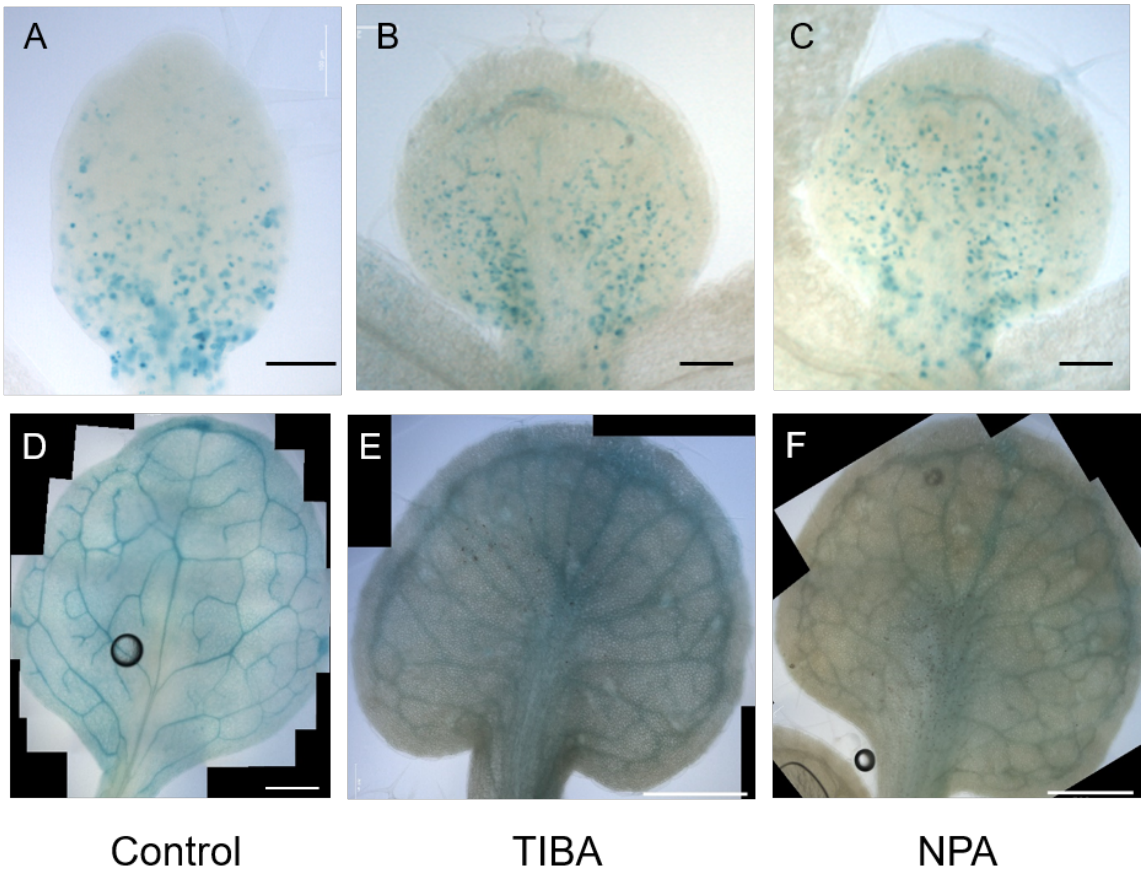

666

667 **Fig. 1** Cell proliferation is visualized by GUS staining in PATI-treated *CYCB1;1::GUS*.

668 A: 6 DAS control, B: 7 DAS TIBA-treated, C: 7 DAS NPA-treated leaf primordia.

669 D: 12 DAS control, E: 12 DAS TIBA-treated, F: 12 DAS NPA-treated leaf primordia.

670 Leaf primordia of similar length were compared.

671 Scale bars: A: 100 µm, B, C: 200 µm, D-F: 500 µm

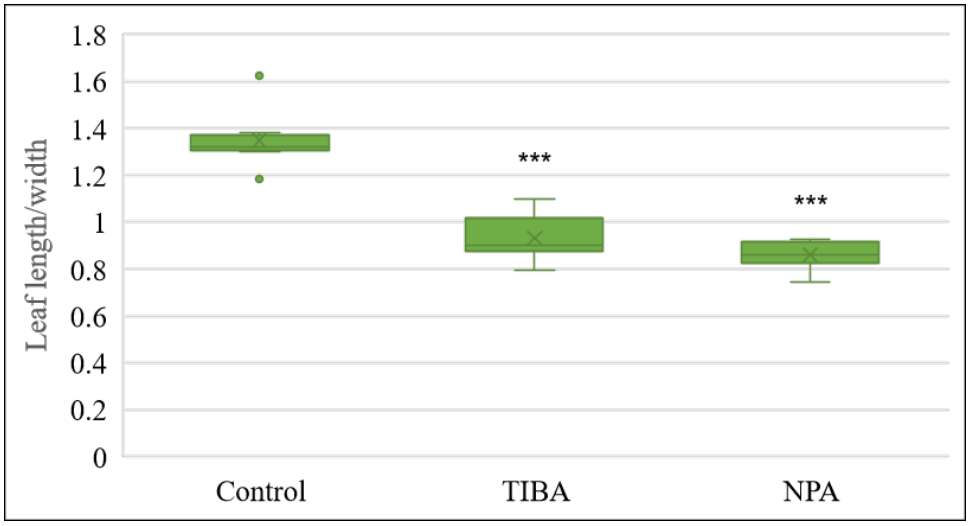

672

673 **Fig. 2** Leaf length/width ratio of leaf primordia at cell proliferation stage.

674 From left to right, data on control, TIBA-treated, and NPA-treated leaf primordia are

675 shown, n = 4, Dunnett's test ***: $p < 0.001$

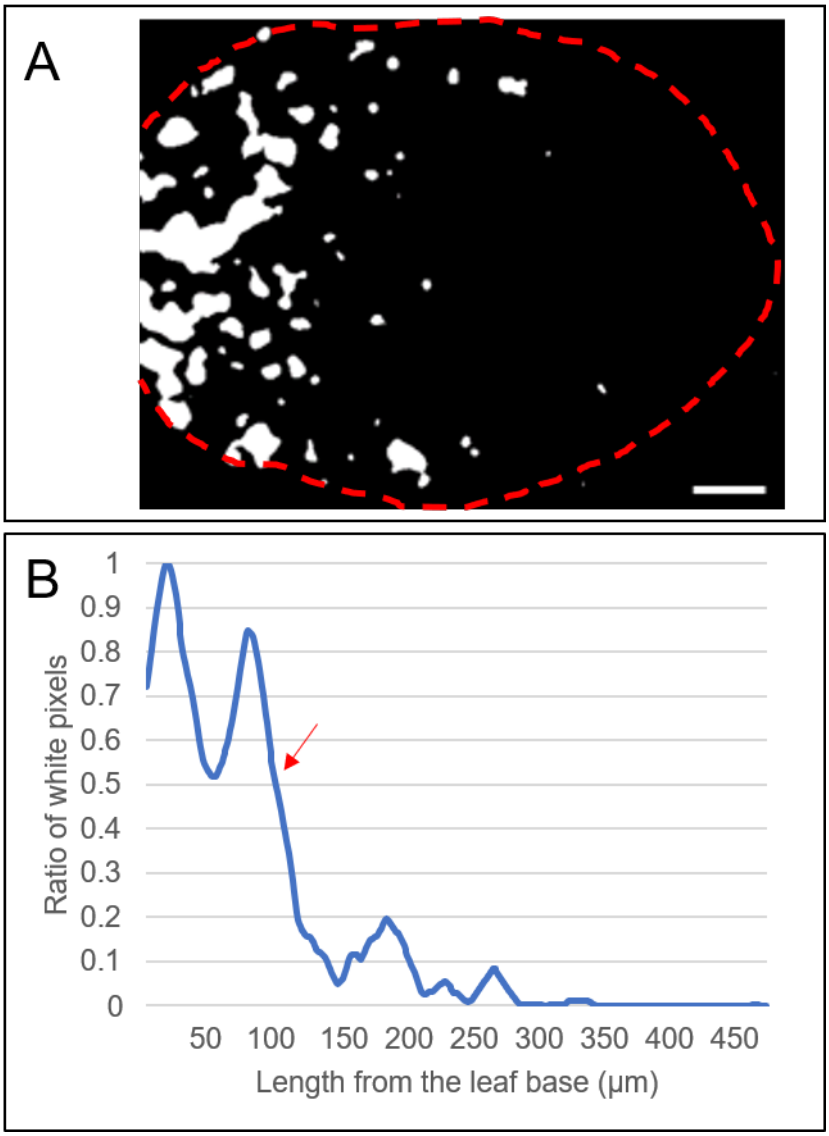

Fig. 3 Determination of cell proliferation zone.

A: Binary images of GUS-stained leaf primordia. Scale bar: 50 μm

B: The ratio of white pixels from a binary image was calculated, and the length of the cell proliferation zone (more than 50% of the white pixels) was determined. The red arrow indicates the end of the cell proliferation zone.

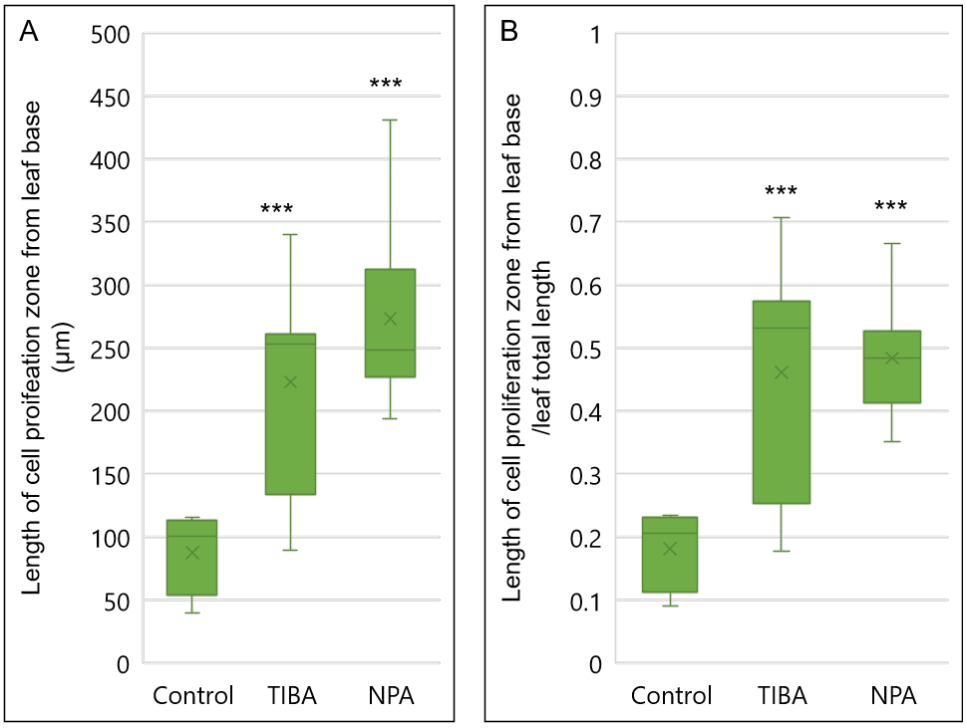

682

683 **Fig. 4** Length and the ratio of cell proliferation occupying leaf primordia.

684 A: Length of cell proliferation zone from leaf base

685 B: The ratio of cell proliferation zone to the total leaf length.

686 n = 8, Dunnett's test, ***: $p < 0.001$

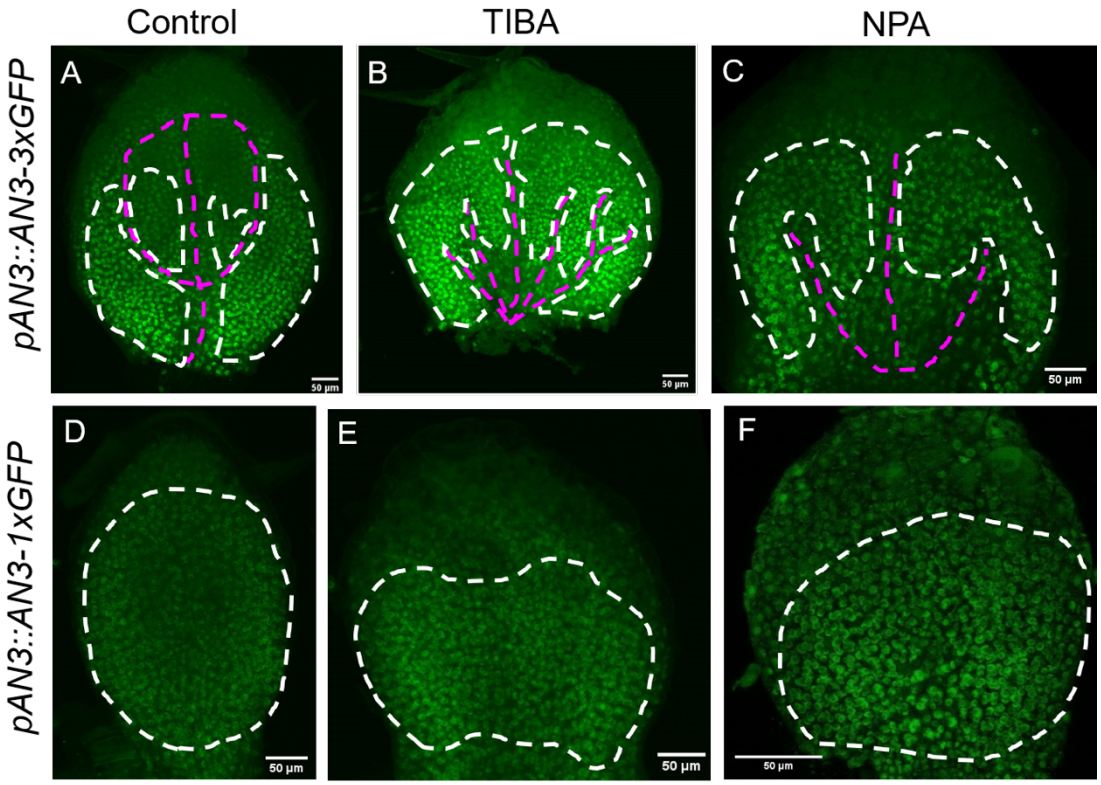

687

688 **Fig. 5** GFP localization of *an3/pAtAN3::AN3-3xGFP* (A-C) and *an3/pAtAN3::AN3-GFP*

689 (D-F).

690 Control (A, D), TIBA-treated (B, E), and NPA-treated (C, F) leaf primordia are shown.

691 White dotted lines indicate GFP-localized area, and magenta lines indicate vasculature.

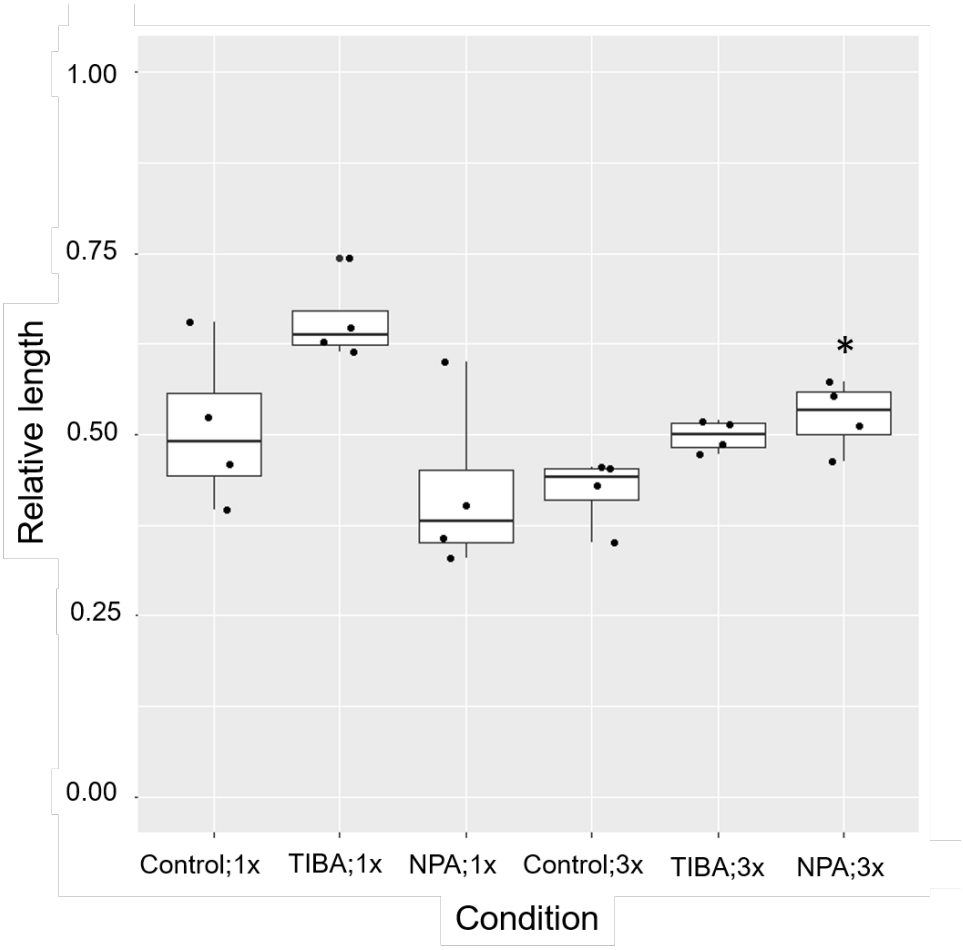

692

693 **Fig. 6** Ratio of AN3 mRNA and protein-localized area to the total length of leaf primordia.

694 From left, *an3/pAtAN3::AN3-GFP* Control, TIBA and NPA; *an3/pAtAN3::AN3-3xGFP*

695 Control, TIBA and NPA. n = 4, Dunnett's test, *: $p < 0.05$. No mark implies no statistically

696 significant difference was observed.

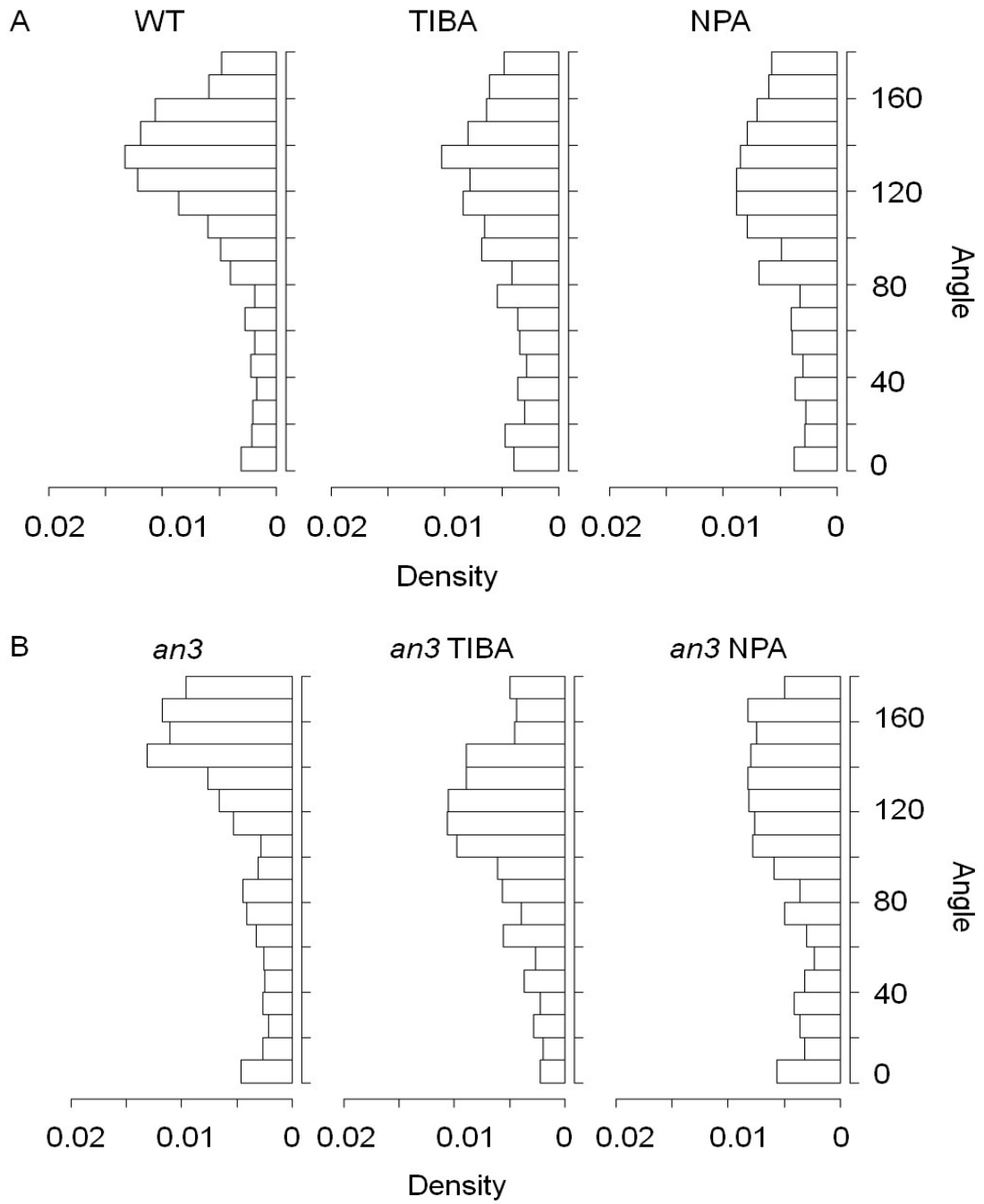

697 **Fig. 7** Cell division angles in leaf and floral organs. Four samples were investigated for

698 each condition.

699 A: From left, WT, TIBA, NPA; 1221, 1158, 1061 pair of cells were analyzed, respectively.

700 B: From left, *an3* mutant, TIBA (*an3* mutant), NPA (*an3* mutant); 971, 703 and 604 pair

701 of cells were analyzed, respectively.

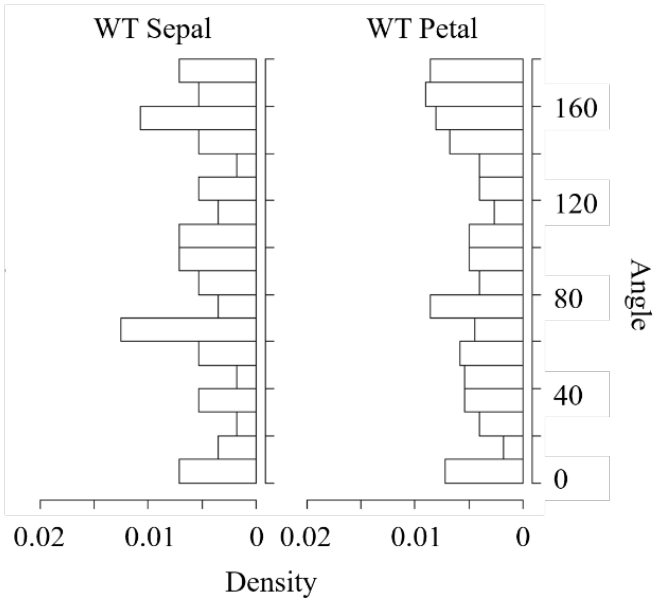

Fig. 8 Cell division angles in floral organs. Four samples were investigated for each condition. From left, WT sepal, WT petal; 56 and 222 pair of cells were analyzed, respectively.

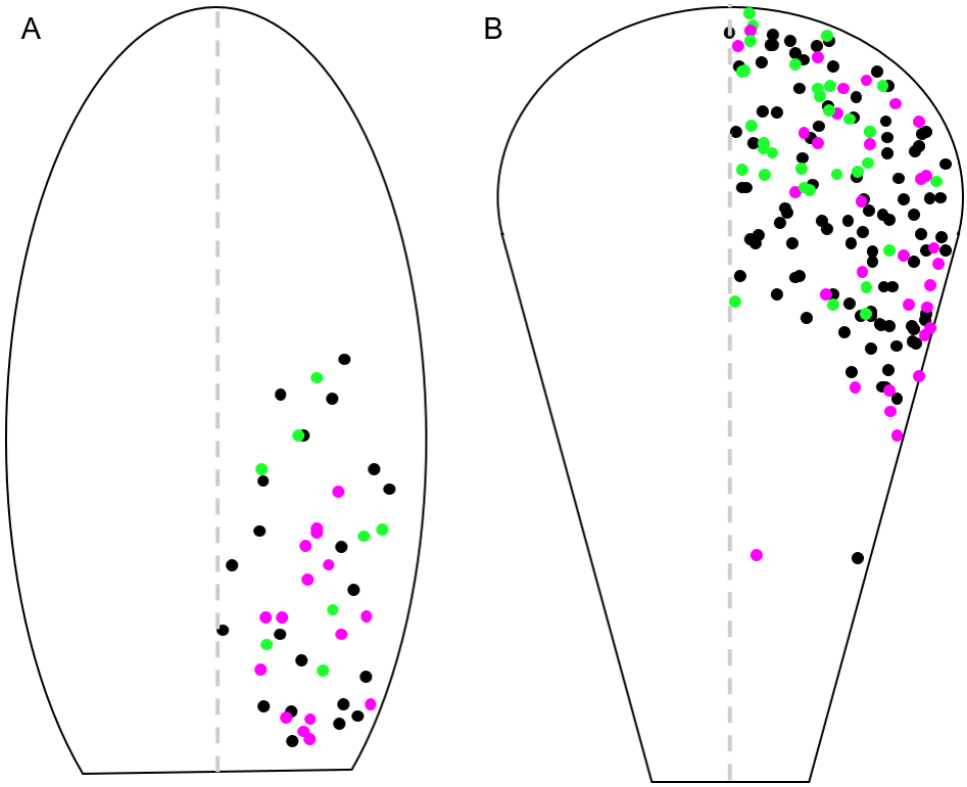

Fig. 9 Cell division angle distribution in floral organs. The angles are mapped to the right half of the diagram, as the organs are symmetrical.

The magenta dots indicate the cell division angle in 180°–140° (the upper peak in Fig. 8), the green dots indicate 90°-60° (the lower peak in Fig. 8), and the black dots indicate the angles that are in neither peak. n = 3. A: Sepal; 46 pair of cells were analyzed. B: Petal; 159 pair of cells were analyzed.

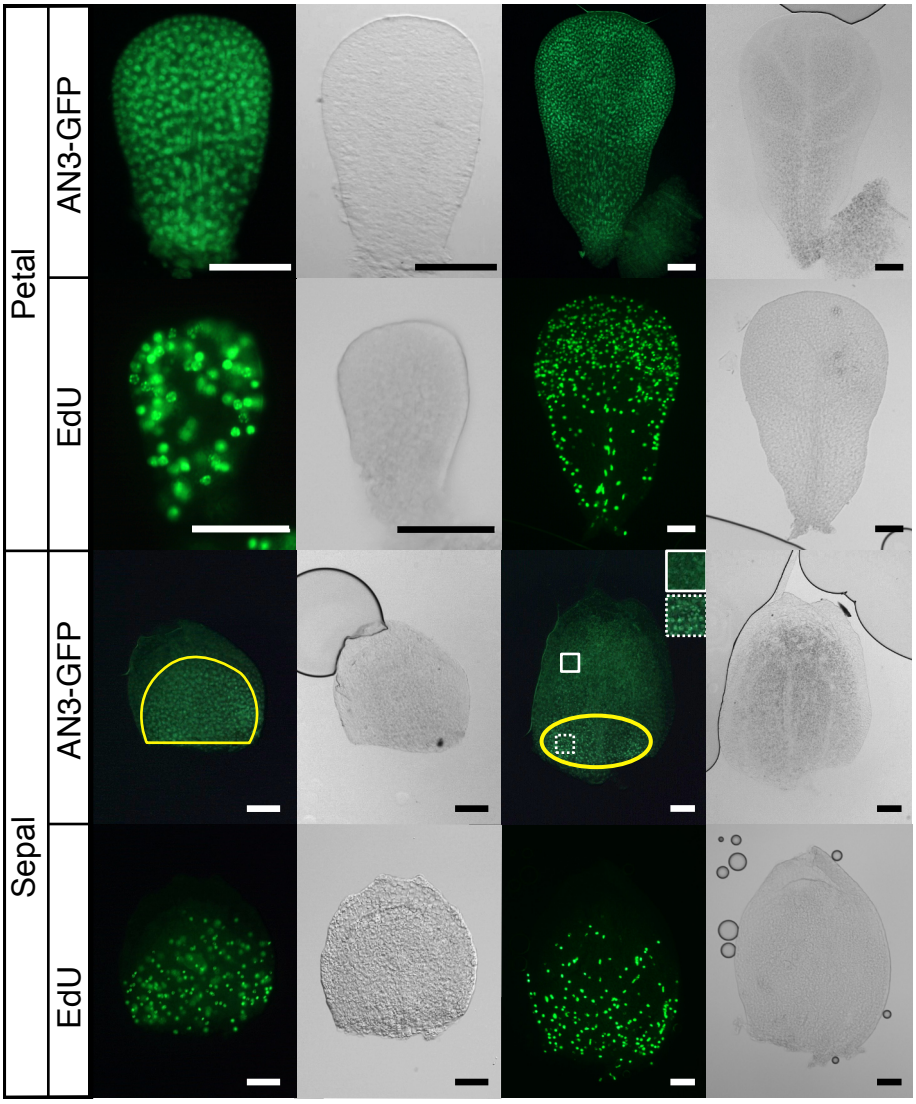

Fig. 10 AN3-1xGFP signals and EdU staining in sepal and petal primordia.

The younger primordia are shown in the left column. Normal transmitted light microscope images are shown on the right side of each fluorescent microscope image. The yellow line shows areas with clear AN3-1xGFP signals. Magnified views in each square of the sepal primordium are shown on the upper right.

Bar = 50 μm

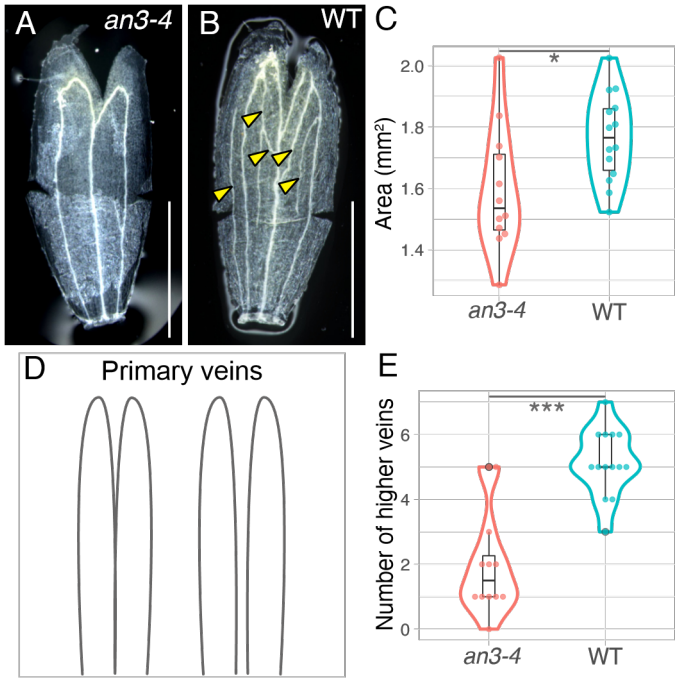

Fig. 11 Phenotype of the sepal in the *an3-4* and the wild type. (A, B) Images of the sepal in each genotype, *an3-4* and the wild type. Some cuts were made to flatten the organs. (C) The area of sepals in each genotype. (D) Two patterns of primary veins defined in this study. (E) The number of higher veins of the sepals in each genotype. * $p < 0.05$, *** $p < 0.001$, Bar = 500 µm